PCCP

Physical Chemistry Chemical Physics

An international journal

www.rsc.org/pccp

Volume 7 | Number 19 | 7 October 2005 | Pages 3385–3508

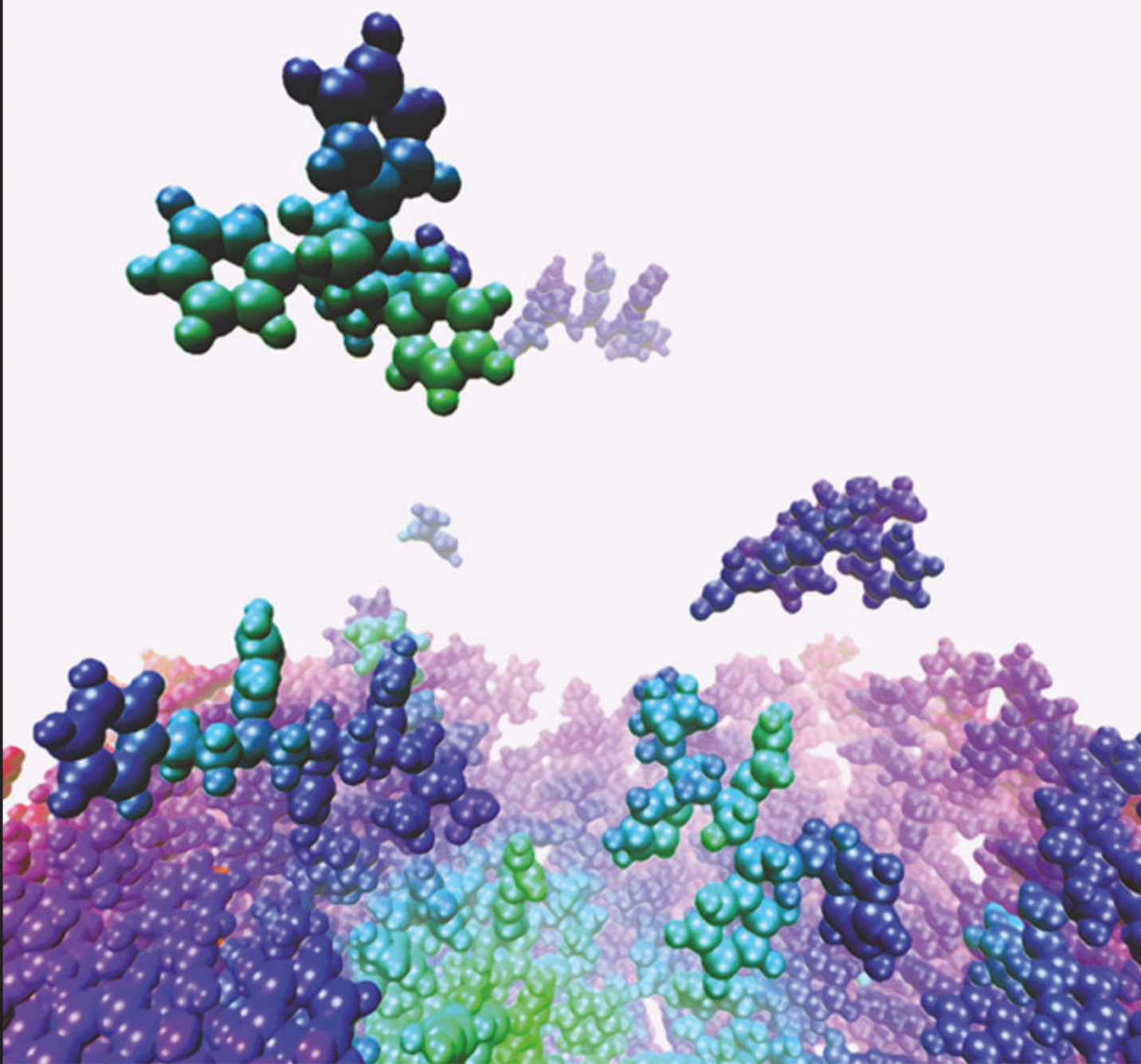

ISSN 1463-9076

INVITED ARTICLE
Delcorte
Organic surfaces excited by low-energy ions: atomic collisions, molecular desorption and fullerenes

HOT PAPER
Uhrín *et al.*
Conformation of glycosaminoglycans by ion mobility mass spectrometry and molecular modelling

1463-9076(2005)7:19;1-R

Front cover

Phys. Chem. Chem. Phys., 2005, **7**(19), 3385
DOI: 10.1039/b512604p

Phys. Chem. Chem. Phys., 2005, **7**(19), 3387

Invited Article

Organic surfaces excited by low-energy ions: atomic collisions, molecular desorption and buckminsterfullerenes

Arnaud Delcorte, *Phys. Chem. Chem. Phys.*, 2005, **7**(19), 3395
DOI: 10.1039/b509238h

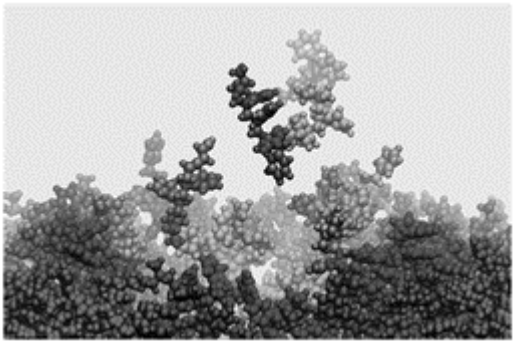

Molecular dynamics and mass spectrometry elucidate the mechanisms of molecular emission from organic surfaces bombarded by monoatomic and fullerene ions.

INVITED ARTICLE

PCCP
www.rsc.org/pccp

Organic surfaces excited by low-energy ions: atomic collisions, molecular desorption and buckminsterfullerenes

Arnaud Delcorte

PCPM, Université Catholique de Louvain, Croix du Sud 1, B-1348 Louvain-la-Neuve, Belgium

Received 29th June 2005, Accepted 5th August 2005
First published as an Advance Article on the web 24th August 2005

This article reviews the recent progress in the understanding of kiloelectronvolt particle interactions with organic solids, including atomic displacements in a light organic medium, vibrational excitation and desorption of fragments and entire molecules. This new insight is the result of a combination of theoretical and experimental approaches, essentially molecular dynamics (MD) simulations and secondary ion mass spectrometry (SIMS). Classical MD simulations provide us with a detailed microscopic view of the processes occurring in the bombarded target, from the collision cascade specifics to the scenarios of molecular emission. Time-of-flight SIMS measures the mass and energy distributions of sputtered ionized fragments and molecular species, a precious source of information concerning their formation, desorption, ionization and delayed unimolecular dissociation in the gas phase. The mechanisms of energy transfer and sputtering are compared for bulk molecular solids, organic overlayers on metal and large molecules embedded in a low-molecular weight matrix. These comparisons help understand some of the beneficial effects of metal substrates and matrices for the analysis of molecules by SIMS. In parallel, I briefly describe the distinct ionization channels of molecules sputtered from organic solids and overlayers. The specific processes induced by polyatomic projectile bombardment, especially fullerenes, are discussed on the basis of new measurements and calculations. Finally, the perspective addresses the state-of-the-art and potential developments in the fields of surface modification and analysis of organic materials by kiloelectronvolt ion beams.

1. Introduction

Ion beams are used for a wide range of applications encompassing surface modification and etching,[1–3] nanometer-scale 3-D patterning (focused ion beams, FIB[4]), controlled deposition of multielemental layers[5] and sub-micrometer scale FIB-induced deposition.[6] When coupled with mass spectrometry, the process of sputtering (*i.e.* the projectile-induced emission of matter in the gas phase) can be used for elemental in-depth analysis and molecular surface characterization (glow discharge mass spectrometry, GDMS, and secondary ion mass spectrometry, SIMS).[7,8] All these methods can be divided in two regimes of ion fluence. The techniques of surface modification and depth-profile analysis (dynamic SIMS) usually involve ion fluences larger than 10^{14} primary ions cm^{-2}. In contrast, molecular analysis of the surface requires low ion fluences, below 10^{13} ions cm^{-2}, so that virtually every projectile samples a fresh area of the surface. Using kiloelectronvolt monoatomic ions, such as Ar^+ and Ga^+, the damage front created by the projectile prevents the retention of the molecular information upon erosion of the target (depth-profiling), a particularly regrettable effect in the case organic materials. However, with the advent of polyatomic ion sources, depth profiling has also been successfully achieved for a series of organic samples, because these projectiles involve a different physics (see section 5).[9–11] In general, polyatomic ions such as SF_5^+,[12] Au_n^+,[13] and C_{60}^+,[14,15] open a new realm of performance for ion beam-based surface analysis and imaging techniques,[16] especially in the field of organic materials.

The understanding of monoatomic and polyatomic projectile interaction with organic and multicomponent materials, however, may still be improved. Unraveling the dynamics of ion penetration, energy transfer, fragmentation and induced desorption in complex samples made of (bio)organic molecules and polymers or samples mixing inorganic particles/substrates with an organic phase, useful in nanotechnology, carries an enormous potential. This is indeed the way to control ion implantation, induced chemical reactions and to envision new projectiles[17] that may provide improved results for surface modification and analysis.

The methods that can be used for gaining a better picture of ion beam-induced processes are both experimental and theoretical. In general, secondary ion/neutral mass spectrometry (SIMS/SNMS) gives information concerning the sputtered species, their yield, energy and angular distributions and, indirectly, about the structural modification, elemental mixing, fragmentation and chemical reactions occurring in the bombarded solid.[7,8,18] Complementary techniques, such as X-ray photoelectron spectroscopy (XPS) and electron energy loss spectroscopy (EELS),[19] scanning and transmission electron microscopies (SEM, TEM) and near-field microscopies (STM, AFM)[18] have also been instrumental for this purpose. From a theoretical viewpoint, analytical[18,20,21] and numerical [22–24] models exist and they have been extensively used for the description of metal, oxide and other inorganic material sputtering and, to a lesser extent, for organic material desorption under ion bombardment. At this time, the most realistic and powerful method appears to be classical molecular dynamics (MD) modeling, which has been successfully applied to the description of organic molecule emission and fragmentation.[25,26]

The focus of this article is placed on the recent advances in the study of ion interaction with bulk organic materials and adsorbed molecules. For this purpose, the text blends results from experiments, mostly obtained using a time-of-flight (ToF) SIMS instrument, and insights from models, essentially classical molecular dynamics. This combination of methods is illustrated in Fig. 1, which shows the desorption of fragments and molecules induced by keV monoatomic projectiles in an organic sample made of polystyrene oligomers. The snapshots

DOI: 10.1039/b509238h

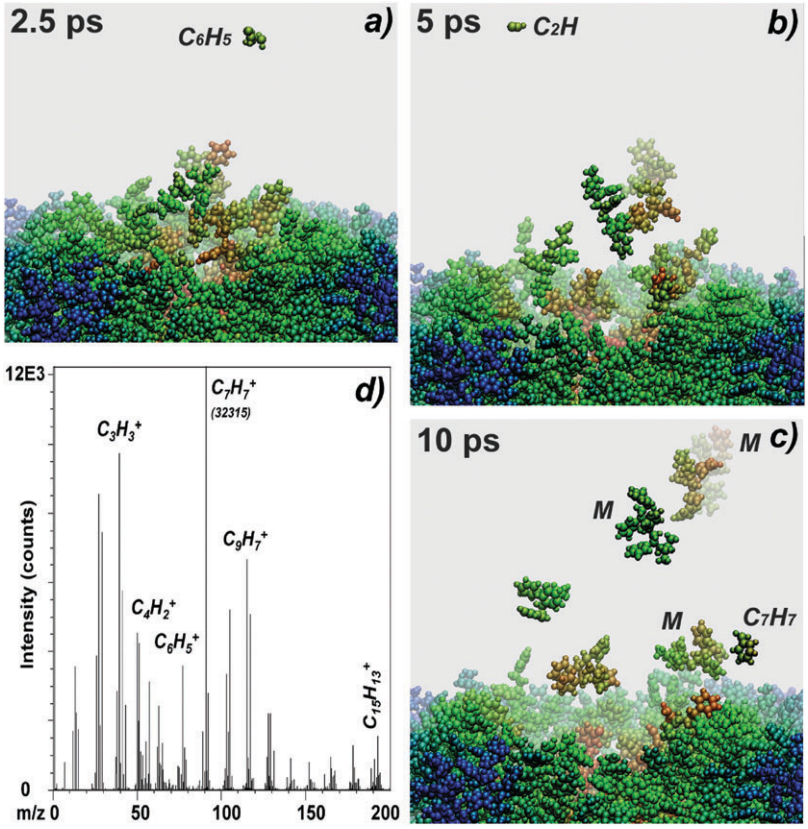

Fig. 1 (a–c) Snapshots showing the time evolution of the molecular dynamics for a polystyrene tetramer solid under 5 keV Ar bombardment (45° polar incidence angle). M signifies the intact polystyrene tetramer molecule. (d) Positive ToF-SIMS spectrum (Ga^+; 12 keV) of a polystyrene film obtained by spin-coating. See ref. 41 for more details.

of the molecular dynamics (Figs. 1a–c) provide a microscopic view of a desorption event, with a detailed chronological description of its successive stages, while the low-mass region of the SIMS spectrum (Fig. 1d) shows the range of ionized fragments sputtered from the surface. Fig. 1 and similar results will be commented in detail along the article. The comparison of experimental and computed results is also informative about the quality of the interaction potentials used in the simulations and the influence of the physics that is *not* implemented in the model, *e.g.* the electronic processes responsible for molecule ionization. The results described in the article, whether they pertain to the MD or to the SIMS arena, concern the low-fluence regime, *i.e.* each projectile sees a fresh, undamaged sample. Cumulative effects involving the repetitive bombardment of the same target area are only mentioned along the text when judged appropriately and, in the case where the development of surface modification methods is explicitly considered. In each section of the article, important results from the literature are also described in order to provide the reader with a more complete view of the field.

2. Theoretical and experimental methods

The simulation of kiloelectronvolt particle-induced sputtering involves at least two different regimes of interaction. The first one, corresponding to the first hundred femtoseconds of the projectile–solid interaction, is a regime of high-energy binary collisions, in which the atoms of the system behave like marbles or billiard balls. This stage of the interaction is reasonably modeled within the binary collision (BC) approximation, using purely repulsive interatomic potentials, such as prescribed in the classical sputtering theory and its implementation in Monte-Carlo algorithms like TRIM[22] and Marlowe.[23] At later times, however, the energies of the projectile and recoil atoms become close to the binding energies in the solid and the disturbed sample resembles a classical beads-and-spring system. This part of the interaction, responsible for a number of observed effects—including polyatomic fragment and intact molecule emission—requires full MD calculations. The correct description of bond scission and bond creation processes, frequent in the particle–solid interaction sequence, constitutes another major requirement. Current molecular dynamics algorithms solve these issues using a sophisticated set of semi-empirical and many-body interaction potentials, from which the energy and forces in the system are calculated. These potentials blend a highly repulsive short-distance wall, mimicking the initial billiard pool, with a more complex function—including a repulsive and an attractive part—at larger distance, for the final beads-and-spring system. In our calculations, the C–C, C–H and H–H interactions are described by the AIREBO potential.[27] This potential is based on the reactive empirical bond-order (REBO) potential developed by Brenner for hydrocarbon molecules[28–30] and includes non-bonding intermolecular interactions through an adaptative treatment that conserves the reactivity of the REBO potential. At each timestep of the simulation, the forces between the different constituents of the system are calculated from the atomic positions and the interaction potentials. Then Hamilton's equations of motion are integrated to determine the position and velocity of each particle at the following timestep.[31,32] It is important to remember that electronic excitations and charge exchange processes are not described by the model, which is classical in nature. Therefore, one should be particularly careful when comparing simulation results to SIMS data. However, the effect of the valence electrons in the bonding chemistry is implicitly taken into account *via* the interaction potentials. The MD studies addressing sputtering of metallic/inorganic samples have been recently reviewed[33] and specific reviews on the energetic particle interactions with hydrocarbon and thiol molecules adsorbed on metals are also available.[25,26] Attempts at modeling bulk organic samples are less numerous, because

of their complexity, the limited set of interaction potentials and the required amount of computer time. Among those reports, one notes the study of a polyethylene crystal,[34] a benzene crystal,[35] benzene multilayers on Ag,[36,37] a large (7.5 kDa) polystyrene adsorbate,[38,39] kilodalton polystyrene molecules in a low molecular weight matrix[40] and a polystyrene oligomer solid.[41]

In time-of-flight secondary ion mass spectrometry, the surface of the sample is bombarded by a low-current, pulsed ion beam with a kinetic energy usually comprised between 5 and 25 keV.[7,8] After their emission, the secondary ions are evenly accelerated to a kinetic energy of several keV and their time-of-flight to the detector is measured, with the start time given by the primary ion pulse. The secondary ion masses are derived from the measured time-of-flights. The main factors influencing the time (mass) resolution are the width of the primary ion pulse and the width of the secondary ion initial energy distribution.[42] To compensate for the latter, ion mirrors or electrostatic sectors[8,43] are inserted in the secondary ion path, so that fast ions undergo longer trajectories than slow ions for the same mass. Electrostatic sectors are energy dispersive and, therefore, they can also be used to measure initial energy distributions, by placing a narrow slit on their exit side. The time focusing of the primary ion beam is the other essential condition to guarantee mass resolution. In our ToF-SIMS system, a DC beam (pA-nA current) is blanked by a pair of deflection plates most of the time. To create useful ion pulses, the voltage difference on the deflection plates is set to zero for a very short time and the entire cycle is repeated with a kHz frequency. Further down in the ion gun column, an electrodynamic buncher is added to improve time-focusing of the ion pulses onto the sample surface. In ToF-SNMS, the sputtered neutrals are post-ionized by a laser beam directed parallel to the sample surface.[8,44] In specific instruments, it is possible to vary the delay between the ion pulse and the post-ionizing laser pulse. Then, the kinetic energy distributions can be obtained after coordinate transformation of the recorded time-of-flights to the laser beam.[45] The major fundamental results deduced from sputtering and SIMS/SNMS measurements can be found in review articles, for elemental and inorganic targets[8,46,47] and for organic bulk and thin layer samples.[45,48,49]

3. Interaction of keV projectiles with molecular solids and polymers

Under 5 keV Ar bombardment, a molecular solid made of polystyrene oligomers (4 styrene repeat units, $\sim$500 Da) undergoes a variety of processes including intramolecular bond-scissions, vibrational excitation, hydrogen atom transfer, surface disruption and emission of fragments and intact molecules in the gas phase. Fig. 1a–c illustrates the local excitation of the sample surface after bombardment, followed by the desorption of hydrocarbon fragments, such as C_2H, C_6H_5, C_7H_7, and of several PS molecules, in the first ten picoseconds after the projectile impact. The release of organic material in the vacuum is accompanied by the formation of a crater around the impact point. The low-mass range of the positive SIMS spectrum of a similar PS sample, Fig. 1d, mirrors the processes predicted by the model. It displays a large number of peaks corresponding to hydrocarbon fragments with various sizes, *e.g.* $C_3H_3^+$, $C_7H_7^+$ and $C_{15}H_{13}^+$, characteristic of the molecular structure of polystyrene. In addition, the SIMS spectrum tells us that, beside the dynamics of fragmentation and sputtering, there exist charge transfer processes by which a fraction of the molecular species ejected from the surface become ionized. The difference between the positive and negative SIMS spectra and the relative abundance of the observed ions (*e.g.* odd *versus* even electron ions) also indicates that the rules of ionization are very specific.

In sections 3.1 to 3.3, the projectile energy dissipation, the fragmentation and the desorption processes are discussed using comparisons between simulations and experiments. Observations taken from the literature help us broaden the scope of the presented results. In section 3.4, the issue of ionization is briefly addressed.

3.1 Energy dissipation in the solid

As is the case for other types of targets, the first stage of the interaction between a keV projectile and an organic solid is the creation of a collision cascade, *i.e.* a succession of energetic interatomic collisions, involving several generations of recoil atoms and leading to a number of atomic displacements in the microvolume of the sample surrounding the projectile trajectory. The development of collision cascades under keV bombardment of organic targets has been predicted by the classical theory of sputtering[20,21] and they can be computed using BCA codes such as TRIM.[22,50,51] Our molecular dynamics results involving a polystyrene solid substantiate this prediction. The collision trees of Fig. 2 are a direct illustration of collision cascades obtained under 1 and 10 keV Ar bombardment of PS (45° incidence angle). They describe the trajectories of the projectile and recoil atoms moving with a kinetic energy above 10 eV, up to a time of 200 fs after the impact. At that point, the collision cascade is over for the bombardment conditions considered in this study. There are pronounced differences as a function of the projectile initial energy. Under 1 keV; 45° Ar bombardment, the projectile naturally buries at a depth of 15–25 Å under the vacuum–solid interface and the collision cascade involves a small number of energetic recoils. For the same aiming point, the 10 keV; 45° Ar atom induces a much more complex collision tree in the sample. *via* a series of collisions happening 20 Å under the surface, it creates a first network of subcascades, mostly downward-directed. This sequence of collisions causes significant damage in the depth of the sample. Later on, however, a second series of collisions, 30 Å below the surface, deviates the projectile again and produces another beam of upward-directed subcascades. These recoil atoms lead to the fast ejection of two atoms, more than 60 Å away from the impact point. The projectile finally exits through the side of the simulation cell, with 3.9 keV of kinetic energy, *i.e.* 40% of its initial energy. Provided that the organic sample were larger, one cannot exclude that the remaining energy could cause more upward directed sub-cascades and, possibly, more sputtering far away from the impact point.

Over the first picosecond after the impact, the kinetic energy transported in the solid by the projectile and the recoil atoms is transformed into vibrational energy of the molecules surrounding the collision paths. This effect is best described by mappings of the energy in the sample.[41] Fig. 3 shows color contour plots of the average kinetic energy per cell of $5 \times 5 \times 5$ Å^3 (red square in the top-left frame), 2 ps after the impact of a 500 eV Ar atom with the PS solid surface. The sample is sliced horizontally and the kinetic energies associated with upward and downward momentum are split. In this manner, each pair of plots corresponds to a different depth in the sample, with the top graph representing the cumulated kinetic energy corresponding to upward momentum and the bottom graph, downward momentum. The top left contour plot, which shows the kinetic energy associated with upward momenta in the surface layer of the sample, is expected to correlate with molecular emission.[52]

Several observations can be made concerning the energy mappings of Fig. 3. First, they confirm that, after 2 ps, the collision cascade has completely cooled and that the kinetic energy per atom is low ($<$1 eV), even in the most excited regions of the sample. For this projectile energy (500 eV) and incidence angle (45°), the deposited energy tends to remain in the surface region, as expected from Fig. 2a. The energy

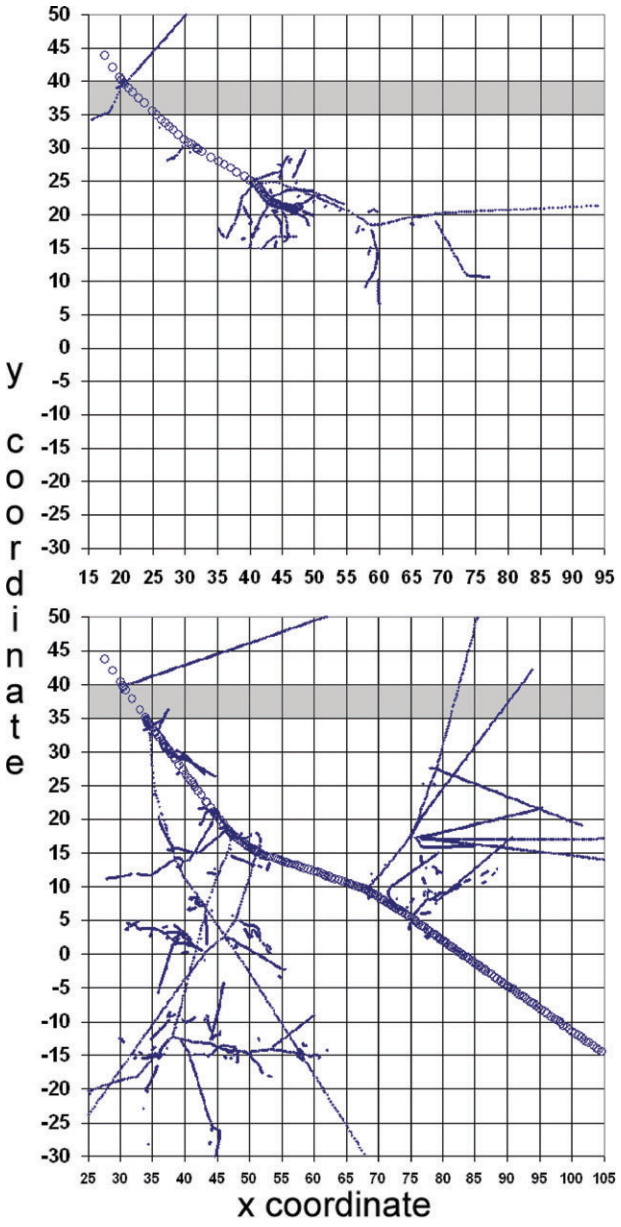

Fig. 2 Tracks of the atoms forming the collision cascade in a polystyrene tetramer solid. The successive positions of the projectile and recoil atoms with more than 10 eV of kinetic energy are represented as a function of time up to 200 fs. The *x* and *y* coordinates are in Å. The sample–vacuum interface is indicated by the gray rectangle. (a) Ar, 1 keV, 45° polar angle (b) Ar, 10 keV, 45° polar angle.

dissipated in the depth of the sample is close to the thermal energy at room temperature (~0.2 eV per sub-cell). Second, the good matching of the "up" and "down" plots for each slice shows that there is no strong orientation of the average momentum, *i.e.* there is a similar amount of energy in downward and upward motion in the sub-cells, which indicates that the motion is largely vibrational. The differences observed, for instance, in the surface region (red arrow), point to molecules having a marked collective upward motion. These molecules are being ejected from the surface. Third, the energy peaks present at the surface but also in the bulk of the sample (white arrow) suggest that the energy remains localized among a subset of molecules, even after 2 ps, a time that is sufficient for the complete randomization of the energy in a metallic target.[41,52] This effect has been explained by the weak coupling between intramolecular and intermolecular vibration modes in the molecular organic solid.[41] This analysis supports an emission process induced by the vibrational excitation of the surface molecules and their interaction with the surrounding medium, somewhat analogous to a local heating of the sample.

3.2. Fragmentation of organic molecules

Understanding organic sample fragmentation upon kiloelectronvolt ion bombardment is the key for the interpretation of secondary ion mass spectra. Therefore, it has been widely investigated by the SIMS community.[53] Most studies are based on the analysis of peak patterns and the application of chemistry rules from conventional mass spectrometry.[54] A series of works elegantly used the collision-induced dissociation of molecules and fragments in the gas phase to model the processes occurring upon emission (tandem MS).[55–58] The analysis of ion-beam damaged surfaces provides another source of information.[58–60] A fourth option concerns the study of the kinetic energy of the sputtered fragments.[48,61–63] Because of the chosen experimental method (SIMS/SNMS), the conclusions concerning processes occurring in the sample are indirectly drawn from the observation of the sputtered species.

Several effects have been reported when comparing the kinetic energy distributions (KED) of organic fragments and molecular species sputtered from molecular solids and polymers. For hydrocarbon polymers, it was observed that the average kinetic energy of fragments and the extent of the high-energy tail of the KED decrease with their size and their degree of resemblance to the structure of the pristine molecule.[62] The size effect is illustrated in Fig. 4a for a polystyrene sample. The size-dependent decrease of the translational kinetic energy was explained by the parallel increase of the energy stored in the ro-vibrational mode of the sputtered species.[61] The second effect, *i.e.* hydrogen deficient and reorganized fragments have larger kinetic energies, is due to the larger energy transfer needed for their formation, which is also mirrored in the translational energy mode. They essentially result from more violent interactions in the sample surface.[60,64]

Molecular dynamics simulations confirm the higher kinetic energy of very small fragments (C_2H_2) with respect to larger and more characteristic fragments (C_6H_5).[38,65] In addition, they indicate that fragmentation in the surface region, responsible for many of the species observed in the experimental mass spectra, is caused by the projectile itself and by the first few energetic recoil atoms.[38] Fragmentation and atomic displacements in the bulk of the solid, important in the case of energetic monoatomic projectiles as shown by the collision cascade, Fig. 2b, generate free radicals that constitute reactive centers for further reactions.[19,66,67] These include branching and cross-linking reactions,[68,69] dehydrogenation,[59] preferential emission of specific residues,[70] and, for large ion fluences, carbonization.[19] More specific chemical reactions, initially triggered by the hyperthermal energies locally deposited in the region of the collision cascade, have been postulated on the basis of the observed mass spectra.[66,71] Potentially, MD simulations are also capable of describing reactions occurring in the sample surface, such as branching and cross-linking. The study of a polyethylene sample provided indications of such reactions, by showing the presence of C atoms bound to three other C atoms after 1 keV Ar bombardment.[34] The emission of fragments enriched in hydrogen with respect to the polymer stoichiometry also indicated the dehydrogenation of the polyolefin upon bombardment, as was observed in the experiment for similar samples.[59] Hydrogen transfers and molecular rearrangements upon bombardment have also been identified in MD simulations involving a large polystyrene molecule.[38]

Experiments and simulations concur to show that the sputtering of organic materials and polymers generates a population of relatively excited molecular fragments. A significant fraction of them has a sufficient internal energy to undergo unimolecular dissociation over the microseconds following the emission. Experimentally, daughter ions produced in the field

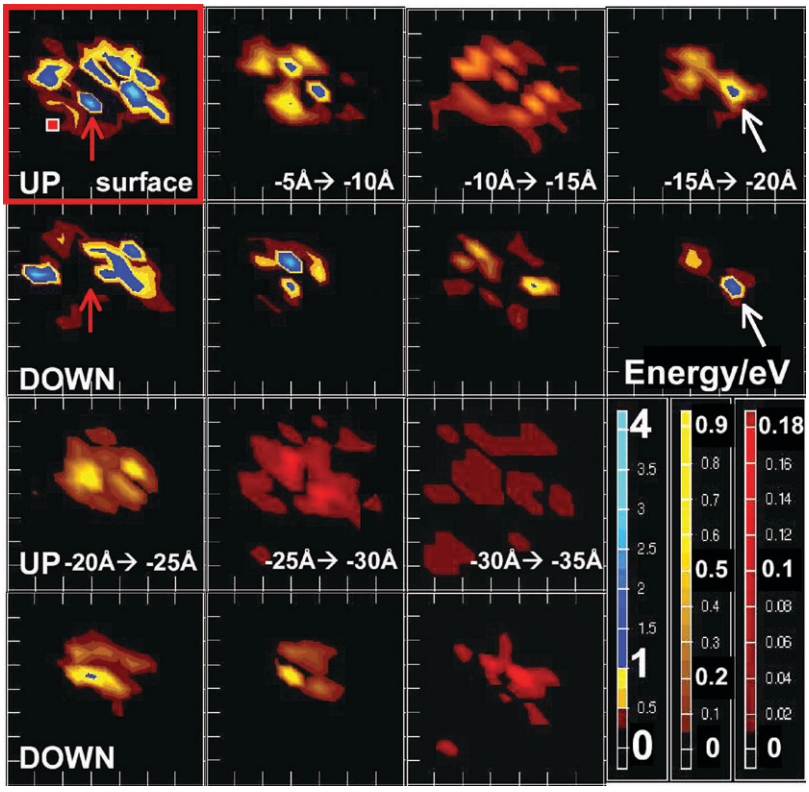

Fig. 3 Kinetic energy distribution in a polystyrene tetramer sample, 2 ps after the 500 eV Ar projectile impact (45° polar incidence angle). Each pair of frames shows the cumulated kinetic energy of atoms with an upward/downward momentum in the $5 \times 5 \times 5$ Å^3 sub-cells (the small red square in the top left frame indicates the area of a sub-cell). For the signification of the red and white arrows, see text. The energy scale on the right side of the figure is in eV. Adapted from ref. 41.

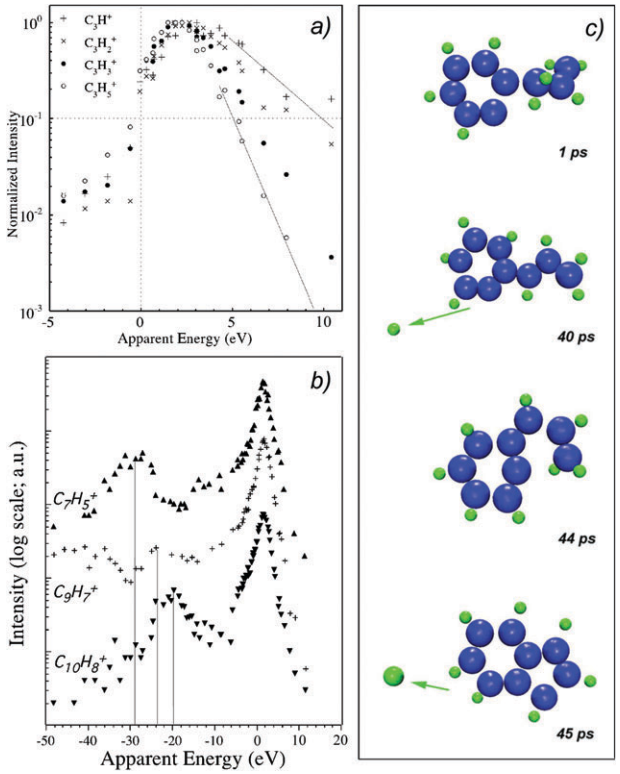

Fig. 4 Fragmentation of a polymer target. (a) Experimental energy distributions of $C_3H_y^+$ fragments sputtered from high-molecular-weight polystyrene bombarded by 12 keV Ga^+ ions. (b) Energy distributions of aromatic fragments. The negative apparent energy corresponds to ions with an energy deficit with respect to the full acceleration energy provided by the spectrometer. (c) Rearrangement and unimolecular dissociation of an excited C_9H_9 fragment after emission (MD simulations). Adapted from ref. 72.

free drift region of a ToF spectrometer with electrostatic sectors constitute a well-defined peak in the measured energy distribution. The peak position in the KED corresponds to a deficit with respect to the total (acceleration + initial) kinetic energy that is directly proportional to the mass of the lost neutral.[48,72,73] As an example, Fig. 4b shows the KED of three aromatic ions observed in the positive SIMS spectrum of polystyrene. On the left of the main peak of the KED, in the "negative" region of the spectrum (corresponding to an energy deficit with respect to the full kinetic energy provided in the acceleration of the spectrometer), one notices a secondary peak that can be attributed to the loss of one H atom by the excited precursor ion. In the case of $C_9H_7^+$, there is also a broad third peak that is due to the loss of 2 and possibly even 3 hydrogen atoms. Such reactions involving (multiple) H atom losses could be isolated in the MD simulations, by running extended time calculations for the ejected species. Fig. 4c illustrates the different stages of the reorganization reaction for an excited C_9H_9 fragment sputtered from PS. About 40 ps after emission, the C_9H_9 fragment releases two H atoms in a time interval of 5 ps, the ejection of the second one being accompanied by the closing of a five C atom ring, eventually forming a very stable two-ring aromatic structure (C_9H_7). The delayed fragmentation, on the surface, of a large polystyrene molecule excited by a 500 eV projectile has also been described in a previous report (see Fig. 9 in ref. 38).

3.3. Desorption of intact molecules

Experimental results from SNMS[74,75] and SIMS[76] show that the bombardment of thick organic films gives rise to the emission of intact molecules. In many cases, however, they are not observed in SIMS because there is no efficient ionization mechanism (for bulk PS oligomer sample, no intact molecule is observed in the 15 keV Ga^+ SIMS spectrum).

Particle-induced molecular desorption from an organic solid has been illustrated in Fig. 1. The complete scenario can be reconstructed with the information provided by the analysis of Figs. 1–3. In the first picosecond after impact, the energy transported by the collision cascade internalizes in the vibrational modes of the surrounding molecules (Fig. 3). Excited molecules sitting in the surface region gain upward momentum through a "chain" of interactions with the molecules around and underneath them. Eventually, some of these molecules detach from the energized surface, as shown in Fig. 1. Another MD study, considering the bombardment of a benzene crystal by 300 eV Ar atoms, concurs to this general view.[77] In that case, molecules neighboring the region directly fragmented by the projectile and the fast recoils, are set in motion without damage, some with an upward momentum. For these small and stiff molecules, however, the authors notice that the initial atomic collision cascade is followed by a molecular cascade, where the benzene units act as "superatoms". Experiments conducted with benzene upon 8 keV; 45° Ar^+ bombardment, show that benzene molecules can still be desorbed when the benzene layer is covered by a film of *sec*-butyl alcohol molecules (40 Langmuir exposure).[78] This observation indicates that, for a weakly bound molecular solid, the thickness of the volume desorbed by keV ions corresponds to several monolayers.

3.4. Ionization of an organic sample

Kiloelectronvolt particles penetrating an organic solid create excited electronic states and ionized species along their track, *via* hard nuclear collisions and interactions with the electron cloud of the target atoms. It was estimated that a 10 keV Xe projectile generates about 70 ionizations in an organic medium.[79] Because of the insulator character of most organic samples, the ionized and excited states are long-lived and a fraction of them can be transferred in the vacuum within the sputtered material. Charge exchange processes occurring upon ejection give rise to an additional population of secondary ions. The mechanisms, however, are various, sample specific and difficult to model. Many molecules, especially polar species like amino acids[80,81] and amphiphile molecules,[82] ionize through the addition or loss of a proton, forming $(M - H)^-$ and $(M + H)^+$ parent-like ions. As a function of their acid/base character they tend to aggregate with a cation or release a proton upon ejection. Aromatic molecules often form positive ions *via* the loss of an electron.[83] Under certain conditions, molecules also ionize according to their partial charges in the surface, *i.e.* there is already an ion precursor[84] or preformed ion[85] before the projectile impact. Electron impacts above the surface, inducing electron capture and loss processes, have also been proposed to explain the formation of molecular odd-electron ions.[86] Based on a combination of experiments, MD simulations and *ab initio* calculations, it was also shown that de-excitation *via* electron ejection (thermoionic emission), previously proposed for metallic clusters,[87] was energetically possible for organic molecules.[88]

4. Large molecule desorption: substrate and matrix effects

The sputtering and ion formation mechanisms of a surface organic molecule excited by an energetic particle strongly depend on the local chemical environment. This is called the matrix effect.[89] The dynamics of the collision cascade and energy transfer processes, not to mention the ionization mechanisms, are affected by the nature of the underlying substrate (*e.g.* organic *versus* metallic film) and by the strength of the interaction between the molecule and its environment (*e.g.* binding to the substrate, crystallinity, hydrogen bonding). The two cases of the metal substrate and the low-molecular-weight organic matrix are considered hereafter.

4.1. Molecules on a metal substrate

The procedure of casting organic molecules on a metal substrate such as Cu, Ag and Au immediately found a wide range of applications in static secondary ion mass spectrometry.[90–93] Indeed, the charge transfer processes facilitated by the metal substrate induce the emission of ionized molecules that cannot be detected otherwise. Some molecules directly ionize through electron transfer with the surface while others recombine with a metal atom/ion (the exact process is not yet clear, see hereafter). The second important effect of the metal substrate is to provide a dense, heavy crystalline medium in which the dynamics of the projectile penetration and energy dissipation are very different from those depicted in the case of bulk organic solids.[25] In turn, the yields and energies of the ejected molecules are different. The influence of a metallic Ag substrate on the KED of sputtered PS molecules is illustrated in Fig. 5. The first frame shows the agreement between the experimental and

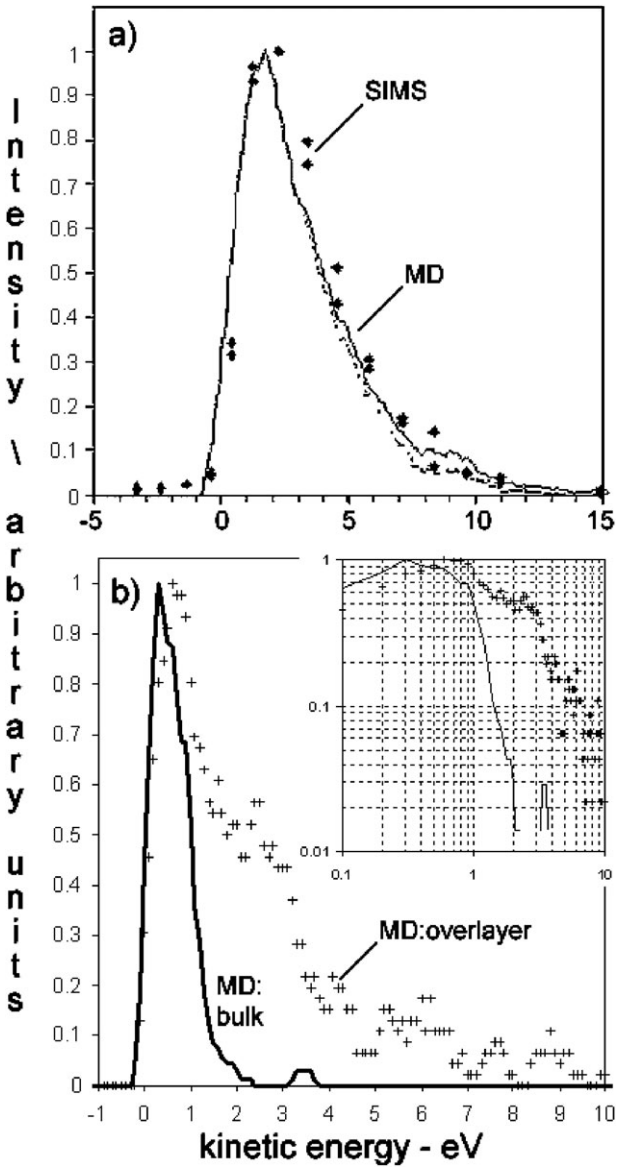

Fig. 5 Kinetic energy distributions of sputtered polystyrene tetramers. (a) PS on a Ag substrate. Comparison between the experimental (12 keV Ga^+ projectiles-diamonds) and calculated (500 eV Ar projectiles-lines) KEDs. The dashed line corresponds to the KED obtained when using an internal energy threshold to discard very excited molecules that are expected to fragment in flight. (b) Comparison between the calculated KEDs of molecules emitted from an overlayer of PS tetramers on Ag{111} (crosses) and from a bulk PS tetramer sample (full line), under 500 eV Ar bombardment (45° polar incidence angle). Adapted from refs. 41 and 65.

calculated results, which confirms that the model adequately describes the interactions at play. The issue is not trivial because, while the interaction potentials within the organic molecules and inside the Ag crystal are very sophisticated, the interaction between the organic molecule and the metal is "simply" modeled by Lennard-Jones functions. The energy distribution of the PS molecules sputtered from a metal substrate is quite broad, with a high-energy tail extending beyond 10 eV. It points to an energetic, collision-induced emission mechanism, far from thermal evaporation. The second frame compares the calculated KEDs of PS molecules sputtered from an Ag substrate and from the bulk PS solid mentioned before, both upon 500 eV; 45° Ar bombardment. The energy distribution of the molecules sputtered from the organic solid is much narrower, in agreement with a softer emission process, that is, the vibrationally-induced desorption described in the preceding section. Experimentally, the reduction of the KED width when going from a monolayer coverage on metal to a multilayered sample has been elegantly demonstrated by Meserole *et al*. for benzene and phenol molecules under 8 keV; 45° bombardment.[75] Using state-selective ionization, the same authors show that vibrationally excited benzene molecules are selectively emitted from the topmost layers of the sample, in contrast to ground-state molecules, which can originate either from the surface or from buried layers.[78]

A closer look at the microscopic level reveals the effect of the metallic substrate on the emission process. Fig. 6a–d gathers snapshots from the molecular dynamics illustrating two extreme scenarios of molecular emission from a layer of PS tetramers (0.5 kDa) adsorbed on silver, under 500 eV Ar bombardment.[65] In the first scenario, Fig. 6a–b, the molecule is essentially hit and pushed upward by an isolated silver recoil atom with a kinetic energy of 12.5 eV. In the second scenario,

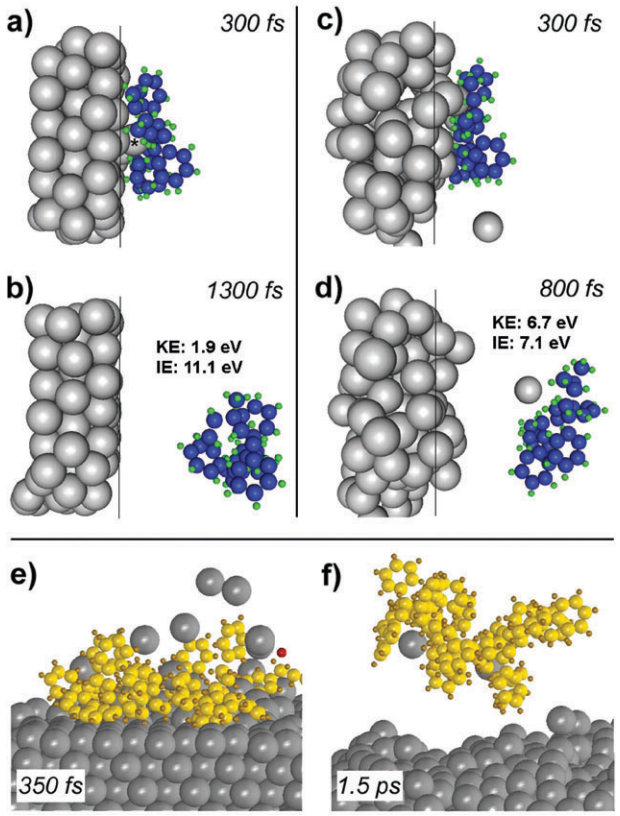

Fig. 6 Scenarios of desorption for molecules adsorbed on a metal (Ag{111}) substrate. (a–b) Single atom-induced desorption of a PS tetramer (500 eV Ar bombardment). (c–d) Cooperative uplifting by several Ag atoms (500 eV Ar bombardment). (e–f) Cooperative uplifting of a PS hexadecamer (16 repeat units; $M_w = 2$ kDa) induced by a 5 keV Ar projectile. Adapted from refs. 65 and 96.

the specific development of the collision cascade in the silver crystal ends up creating a protrusion in the surface, where many silver atoms are collectively moving upwards. The PS molecule is gently lifted up by the cooperative action of at least nine silver atoms with energies in the range 0.5–3 eV. The molecule ejected in the first case absorbs a large fraction of the silver recoil energy in its internal modes (KE: 1.9 eV-IE: 11.1 eV), while the second one gains a comparatively high kinetic energy (KE: 6.7 eV), with relatively little internal energy (IE: 7.1 eV). The cooperative uplifting process also explains the high kinetic energies reported in Fig. 5. In addition, it appears to be the most appropriate mechanism to desorb "cool" organic molecules that have a good chance to remain intact after desorption. The issue is even more crucial for larger, kilodalton (bio)molecules, whose mass and stronger anchoring to the surface make them very unlikely to be desorbed intact by a single recoil atom. This is the case of larger PS oligomers such as the hexadecamer (16 repeat units) displayed in Fig. 6e–f. The simulations show that, in some trajectories, 5 keV Ar atoms are able to create a high action region in the crystal surface, which generates a large-scale collective upward motion of silver atoms. Such mega-events[26] are responsible for the ejection of large intact molecules (Fig. 6f) as well as metallic clusters.[94,95] They are caused by the development of a dense collision cascade, with overlapping sub-cascades, in the surface region of the metal substrate.[96]

The structure of the molecular layer and the binding energy of the molecules to the substrate significantly influence the outcome of the sputtering process. In the case of self-assembled layers of alkanethiols, chemisorbed on noble metals, SIMS experiments show that a wide range of organometallic clusters are ejected from the surface.[97–99] The process is illustrated in Fig. 7, with two snapshots of a MD trajectory obtained under 8 keV Ar bombardment of a layer of octanethiols assembled on a Au(111) crystal.[100] The vertically sliced sample highlights the important action in the energized region of the gold crystal surface. Not long after the collision cascade cooling (Fig. 7a), a few gold atoms are moving upwards in the organic layer. One of them (green rectangle) pulls and unzips a neighbor octanethiol molecule, giving rise to a free gold-thiolate cluster. Larger aggregates are usually emitted at later times, such as the M_2Au_2 cluster (M is the thiolate molecule) marked by the orange rectangle in Fig. 7b, which eventually detaches from the surface around 4 ps (inset). If the aggregation of metal atoms and thiol molecules seems to be caused by the particularly strong interaction between gold and sulfur, it is still the high action unfolding in the surface region of the Au crystal that triggers (supra)molecular emission, as observed for physisorbed PS molecules.

4.2. Molecules in a low-molecular weight matrix

Large (bio)molecules embedded in a low molecular-weight (M_w) matrix constitute a specific type of organic material. Recently, the use of an organic matrix as a means to improve molecular ion emission has regained interest in the SIMS community,[101–104] after the success of this sample preparation procedure in laser desorption ionization mass spectrometry (matrix-assisted LDI).[105,106] For instance, significant yields of bovine ubiquitin ($M_w = 8565$ Da) and single-stranded DNA 26-mer ($M_w = 8157$ Da) have been measured upon dissolution of the analytes in a 2,5-dihydroxybenzoic acid matrix.[101] The advantage of the matrix in the dynamics of sputtering is not completely elucidated but its function as a proton donor for analyte ionization has been demonstrated.[101,104] From the microscopic viewpoint, one can understand that large molecules forming a thick film are difficult to desorb intact. They constitute fragile ensembles that are often strongly bound to the surrounding medium, inserted in a crystalline structure (proteins) or forming a network of entangled coils (polymers).

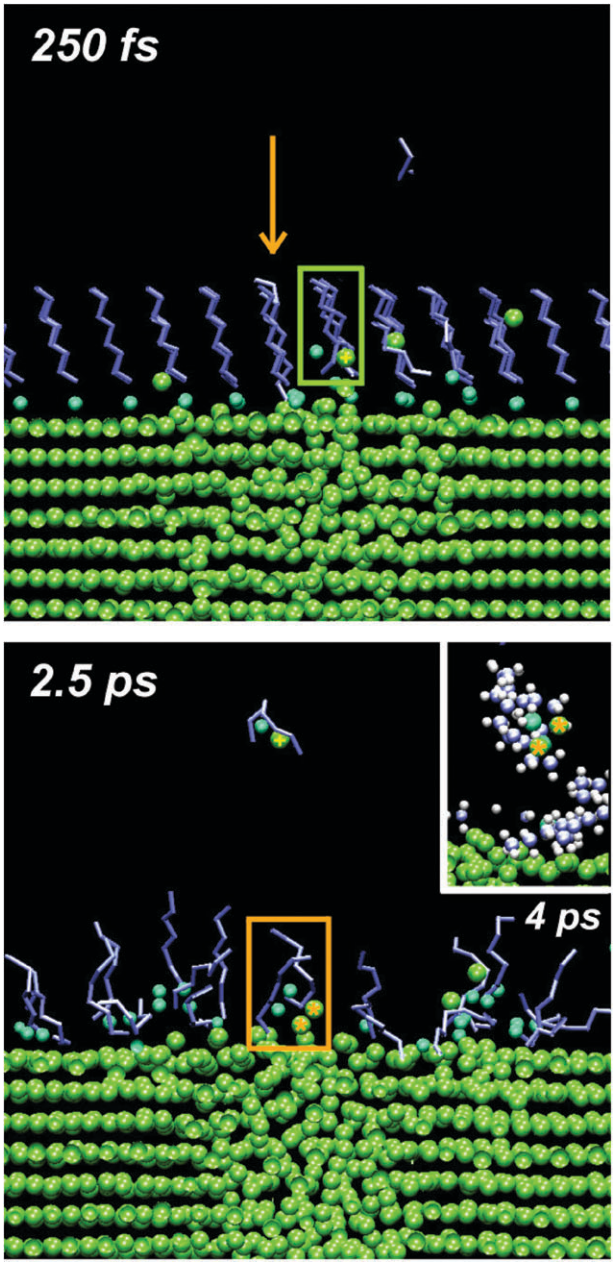

Fig. 7 Mechanism of organometallic cluster emission from an alkanethiol layer on gold under 8 keV Ar bombardment. Movie snapshots through a cross section in the sample illustrating the action occurring at 250 fs (a) and 2.5 ps (b). The orange arrow signifies the aiming point of the projectile. The colored rectangles indicate the nascent clusters. Adapted from ref. 100.

For a polymer such as PS, the limit size for intact desorption from the bulk appears to be close to 3 kDa.[107] In contrast, dilution in a low M_w matrix allows each large analyte molecule to be isolated in a ''nest'' made of smaller entities, with less induced stress upon desorption. To test the effect of a matrix on the desorption process, PS hexadecamers (2 kDa) were embedded in a sample made of trimethylbenzene (TMB) molecules and the effects of 500 eV Ar bombardment were computed.[40] The trajectory movie of Fig. 8a–c shows that the TMB sample surface decomposes under the action of the projectile, releasing one of the PS molecules in the gas phase. Extensive desorption of the surface, already observed for pure benzene targets, is facilitated by the small size of the matrix molecules and the weak cohesion energy of the solid. In the simulations, the desorption process often generates large clusters of matrix molecules and mixed aggregates of matrix molecules associated to a PS molecule. Those clusters, however, do not survive for more than 100 ps after emission. They cool down *via* matrix molecule evaporation.[108]

Experimentally, the positive influence of a matrix on the emission of large oligomers is illustrated in Fig. 8d. A sample of poly-4-methylstyrene (P4MS; $M_n = 3930$ Da) embedded in a tetraphenylnaphthalene (TPN; $M_w = 432$ Da) matrix was metallized with a minute amount of gold (20 nmole cm^{-2}) in order to provide the necessary cationizing agent. In this manner, the cationization of the departing molecules (by gold atoms) is decoupled from the effect of the matrix which, in this case, has no significant influence on the analyte ionization. The bombardment of this sample by 15 keV Ga^+ ions gives rise to a distribution of peaks characteristic of the Au-cationized P4MS oligomers. Large peaks corresponding to the positively charged TPN molecule and its Au-cationized homologue are also present in the mass spectrum. Analyte:matrix clusters are not observed in the SIMS spectrum. It is not surprising, because the instrument records the distribution of ions having survived for several microseconds after emission, *i.e.* long after metastable molecular clusters have decayed, according to the model. To judge the beneficial effect of the TPN matrix, it is important to note that, in contrast to the P4MS:TPN sample, the bombardment of a pure P4MS sample, also covered with gold, does not result in the detection of intact P4MS molecules.

4.3. Substrate and matrix effects on ionization

As mentioned in the text, the presence of a different substrate/matrix has a strong influence on the emission of charged species from the surface. Upon desorption, intact molecules may capture a proton or a metal cation (Na^+, K^+, Ag^+), depending on their chemical environment. The beneficial use of transition metal substrates on molecule ionization has been established very early in the history of organic SIMS.[90,91] A procedure involving the evaporation of small amounts of gold or silver on the organic sample surface has also been proposed.[107] Alternatively, transition and alkali metal salts can be mixed with the sample to achieve cationization.[91,109,110] However, there is still some debate concerning the exact mechanisms and, for instance, recent *ab-initio* studies indicate that ionization might occur upon recombination of the molecule M with a metal atom in an excited electronic state,[111,112] as a result of energy curve-crossing upon interaction. The ionization of organometallic clusters from self-assembled monolayers of alkanethiols on metal (see Fig. 7) seems to be conditioned by the electronegativity of the metal substrate atoms with respect to sulfur.[99] With Ag substrates, clusters of the form M_mAg_n are detected as positive ions when $n = m + 1$ and as negative ions when $n = m - 1$. With less electropositive Au substrates, most of the clusters form negative ions.

5. From monoatomic to polyatomic projectiles

The nature of the incident projectile has a significant influence on the properties of the sputtering event. Recently, high-performance polyatomic ion guns have been designed by several manufacturers and they have been used for experimental investigations as well as analytical purpose.[113] For surface analysis, the main advantage of polyatomic ions, such as Au_n^+ and C_{60}^+, is that they induce a strong, non-linear yield enhancement with respect to monoatomic ions, particularly for thick organic targets.[12–14,114] Therefore, they can be used to improve the low sputtering and ionization yields of molecular and polymeric samples, a prerequisite for complex structural characterization and submicronic molecular imaging.[8] MD simulations and SIMS experiments involving an Ag target concur to indicate that polyatomic projectiles generate a highly excited (superheated) nanovolume in the sample surface, thereby ejecting large chunks of material in the gas phase.[115,116]

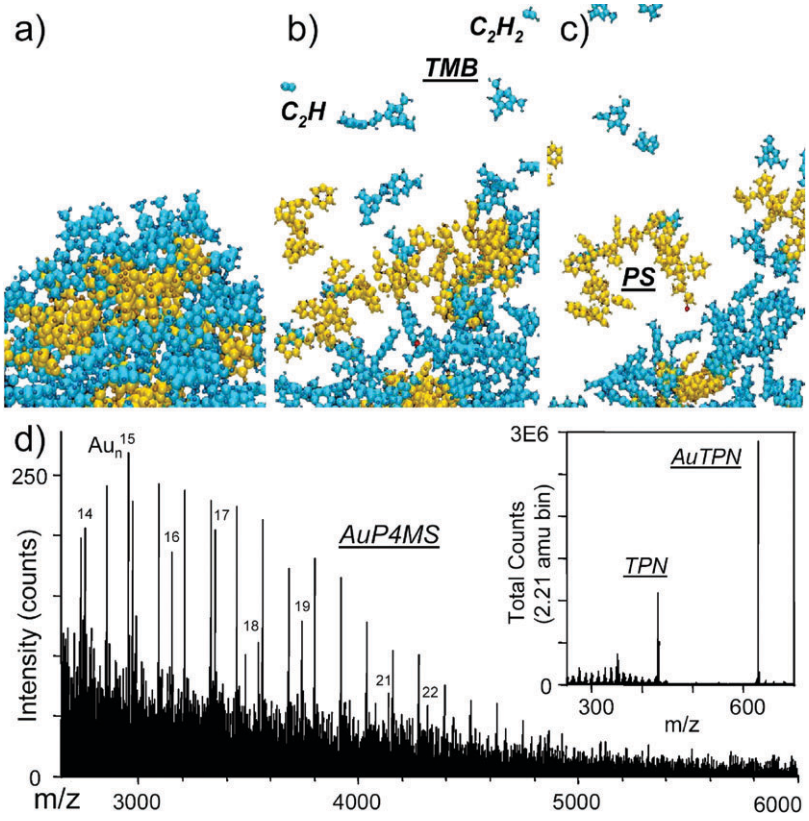

Fig. 8 (a–c) Time-evolution of the molecular dynamics showing the emission of a polystyrene hexadecamer initially embedded in a trimethylbenzene matrix, under 500 eV Ar bombardment. (d) High-mass range of the positive ToF-SIMS spectrum of poly-4-methyl styrene oligomers ($M_n = 3930$ Da) embedded in a tetraphenylnaphthalene matrix ($M_w = 432$ Da), upon 12 keV Ga^+ ion bombardment. The sample was covered with 20 nmol cm^{-2} of gold for cationization. Adapted from refs. 40 and 107.

Their influence on the ionization yield of molecular and fragment species seems to depend on the specifics of the samples.[10–12]

SIMS experiments indicate that, on average, C_{60}^+ projectiles provide the largest yield increases for bulk organic samples.[14] Fig. 9 shows the high-mass range of the positive SIMS spectrum of a thick film of polystyrene oligomers ($M_w = 590$ Da; $M_n = 550$ Da).[117] In sharp contrast with the 15 keV Ga^+-induced sputtering of the same sample (not shown), intact oligomers are detected and they constitute an intense distribution of peaks in the mass spectrum. Complementary measurements involving PS oligomers ($M_w = 1780$ Da; $M_n = 1630$ Da) show that the average ion yield increase with respect to Ga^+ (calculated over the entire mass spectrum), reaches a factor of 120, which reflects reasonably the individual yield increases of the fingerprint ions in the mass range 0–200 Da (140 for $C_7H_7^+$). Similar enhancement factors were reported by Weibel *et al.*[14] Obviously, the ion yield increase is much larger for entire polystyrene oligomers (at least 4 orders of magnitude for short chains, see Fig. 9), since they remain below the detection limit upon Ga^+ bombardment. Very large yield increases are also observed for Irganox molecular ions.[117] In that case, the fact that the Na-cationized molecule displays a 30 times lower yield enhancement than the "bare" molecular ion points to a strong ionization probability enhancement.

It is too soon to propose an exhaustive explanation of the sputtering yield enhancement upon polyatomic projectile bombardment of bulk organic samples. Because of the high action induced in the sample surface by projectiles like C_{60}, realistic MD calculations require significantly larger samples and, in turn, huge computation times. It is possible, however, to describe the first stage of such events, *i.e.* the collision cascade. Indeed, even though the long-term development of the interaction between a 10–20 keV C_{60}^+ projectile and a PS oligomer solid probably requires a sample surface equal or larger than 400 nm^2, *i.e.* thousands of molecules, the containment of the collision cascade, even at 25 keV, can be easily achieved with the sample of Fig. 1 (232 molecules). The collision trees

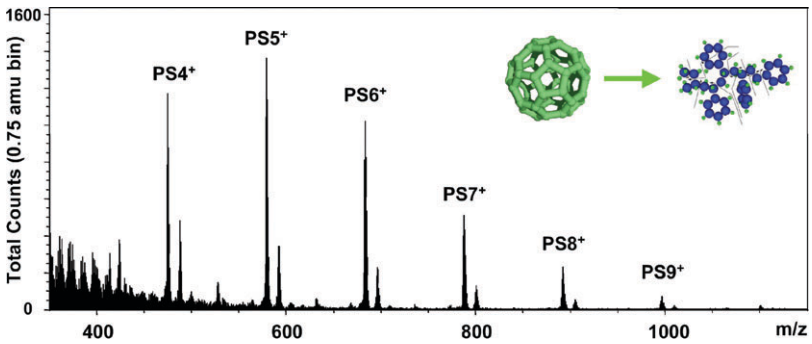

Fig. 9 High-mass range of the positive ToF-SIMS spectrum obtained from a PS oligomer ($M_n = 550$ Da) thick film upon 12 keV C_{60}^+ ion bombardment. Adapted from ref. 117.

computed upon 1 and 10 keV fullerene bombardment of polystyrene are shown in Fig. 10a,b. The tree obtained under 1 keV bombardment (16.7 eV atom^{-1}) is almost limited to the tracks of the C atoms of the fullerene (Fig. 10a). The projectile atoms are buried in the topmost 10–15 Å of the surface, with the creation of very few and low-energy recoil atoms in the solid. Although the effect seems mild when looking at the collision cascade, this quantity of energy deposited by a buckminsterfullerene is sufficient to decompose the whole sample (75 × 75 × 45 Å^3) at later times. Upon 10 keV C_{60}^+ bombardment (166.7 eV atom^{-1}), a larger nanovolume of the organic sample (~20 nm^3) is occupied by the collision cascade (Fig. 10b). The geometry of the collision tree is an ellipsoid, sitting directly underneath the sample surface and its structure is extremely dense, with a large number of overlapping projectile/recoil atom tracks. Preliminary results obtained under 500 eV bombardment of a PS solid show that the energy deposited by the fullerene creates a crater in the sample and induces a collective outward molecular motion. Another MD study involving a larger benzene crystal indicates that 15 keV C_{60} projectiles penetrate significantly into the sample,[118] eventually ejecting molecules *via* a pressure pulse. Studies involving larger molecular samples are in preparation and they should help us gain a more precise view of the fullerene–organic solid interaction.

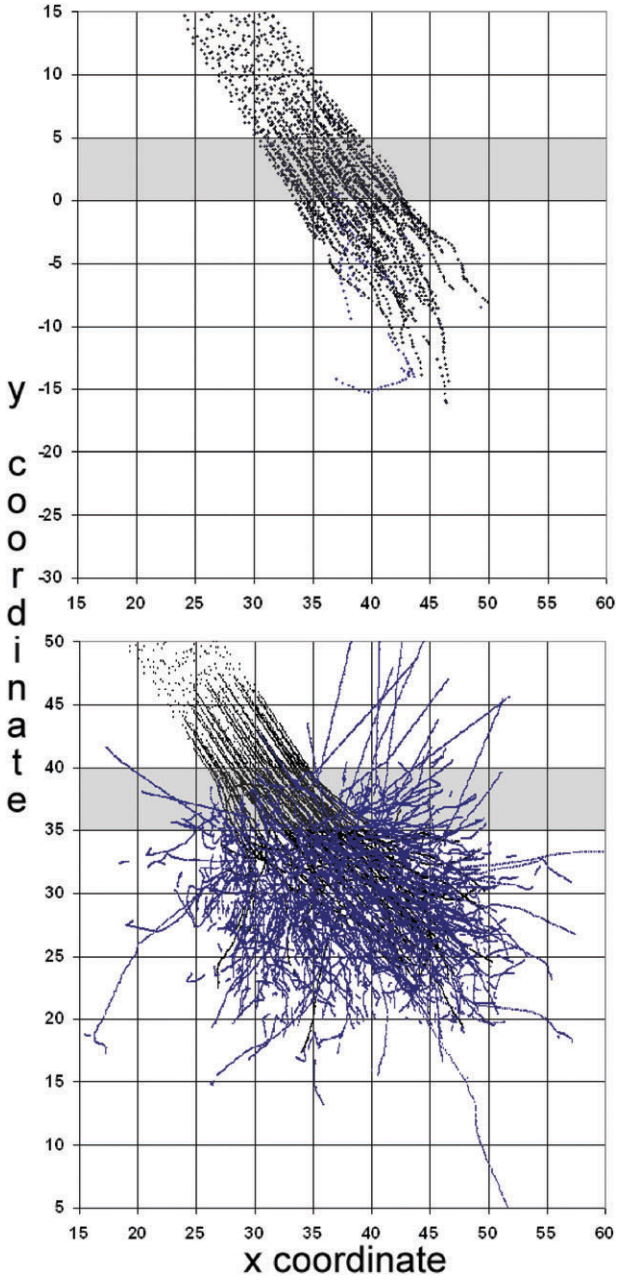

Fig. 10 Collision trees obtained upon fullerene projectile bombardment of a polystyrene tetramer solid. The successive positions of the projectile and recoil atoms with more than 10 eV of kinetic energy are represented as a function of time up to 200 fs. The *x* and *y* coordinates are in Å. The sample–vacuum interface is indicated by the gray rectangle. (a) C_{60}, 1 keV, 45° polar angle (b) C_{60}, 10 keV, 45° polar angle. Adapted from ref. 117.

6. Perspectives for surface modification and analysis with ion beams

In the field of materials science, ion beams have the required properties and the versatility (choice of the projectile nature and energy) to offer solutions to major current technological problems, *e.g.* the design of micro- and nano-objects or the compatibilization of surfaces. In particular, the number of applications of high-current focused Ga^+ beams, very efficient to cross-section and engineer inorganic surfaces with a high lateral resolution (~10 nm),[4] is quickly growing. They are now used for assisted deposition of sub-micronic metal wires (FIBID),[6] preparation of atom probe specimens for characterization[119] or attachment of nanotubes to metal tips,[120] to mention only a few examples. They are able to precisely section organic materials as well.[121] More "traditional" low-energy ion beams (He, Ar) continue to be applied in many processes of organic material engineering, *e.g.* ion beam assisted deposition (IBAD) of molecular films[122] (light emitting diodes[123]), polymer surface modification/patterning[124] for improved peptide adhesion, bone reconstruction,[125] metal adhesion,[126] electrical[127]/optical[128,129] property tuning and waveguide elaboration.[130] Embedded metal cluster layers and metallic nanostructures can be created in an organic matrix using transition metal ion beams[131,132] and metal cluster (20–200 atoms) beams.[133]

For many applications involving organic materials, surface analysis by ion beams (ToF-SIMS/SNMS) demands a higher sensitivity.[8] In this context, there is no doubt that polyatomic primary ions will continue to play a major role in the field. These projectiles have other advantages. For instance, the performance of C_{60}^+ for the molecular depth profiling (dynamic SIMS) of organic samples is outstanding.[10,11,14,134] The tentative explanation is that, because of their limited penetration depth and high energy transfer in the topmost layers of the sample (see Fig. 10), C_{60}^+ ions sputter the damage they create in the surface. New amazing properties of fullerenes are still emerging, *e.g.* the topography induced upon erosion of metallic samples by traditional projectiles does not occur with C_{60}^+.[113,135] One current challenge is to combine high sensitivity and depth profiling capabilities with high lateral resolution, in order to obtain an efficient surface and 3-D molecular analysis technique,[113] able to provide detailed information from complex nanostructures such as those envisioned for molecular electronics, biosensor and tissue engineering applications. In this context, there is also room for other projectiles than fullerenes, first, because the lateral resolution of C_{60}^+ beams is still inferior to that of metal ion guns, for technological reasons. Also, fullerenes might not necessarily be the best option for static SIMS of heavy inorganic materials, bare or covered with a molecular overlayer, as suggested by the limited yield enhancement measured for Ag crystals[115,136] (even though C_{60}^+ beams provide very interesting results for depth profiling such materials, as mentioned above[135]). The moderate yield increase observed for metal surfaces is partly related to the low mass ratio between the projectile and target atoms. In this respect, heavier atoms—and better focused—polyatomic beams, such as Au_n^+ and Bi_n^+, constitute good alternatives.[137,138]

In conclusion, every projectile has its own flavor that, in the ideal laboratory, should be chosen as a function of the

envisioned application. Conversely, it is likely that the discovery of novel projectiles, fueled by experiments and MD simulations,[17] will continue to widen the horizons of surface modification and analysis.[113]

Acknowledgements

I wish to thank Prof. Giovanni Marletta for this invitation to write an article for PCCP. My gratitude also goes to Barbara Garrison from the Pennsylvania State University and Patrick Bertrand from the University of Louvain for their insightful suggestions and continued support. Bahia Arezki provided the simulation results displayed in Fig. 7. The financial contributions of the ''Fonds National de la Recherche Scientifique'' of Belgium and the National Science Foundation of America are gratefully acknowledged. Computational resources were provided by the Academic Services and Emerging Technologies (ASET) of Penn State University. The authors are also thankful to the ASET staff for assistance with the Lion-xe and Lion-xl clusters. The Theoretical and Computational Biophysics group of the University of Illinois at Urbana-Champaign is acknowledged for the development and free access to the visualization software VMD.

References

1 *Ion Beam Modification of Surfaces: Fundamentals and Applications*, ed. O. Auciello and R. Kelly, Elsevier, Amsterdam, 1984.
2 *Ion Beam Modification of Insulators*, ed. P. Mazzoldi and G. W. Arnold, Elsevier, Amsterdam, 1987.
3 Z. W. Kowalski, *Vacuum*, 2001, **63**, 603.
4 J. Gierak, E. Bourhis, M. N. Mérat Combes, Y. Chriqui, I. Sagnes, D. Mailly, P. Hawkes, R. Jede, L. Bruchhaus, L. Bardotti, B. Prével, A. Hannour, P. Mélinon, A. Perez, J. Ferré, J.-P. Jamet, A. Mougin, C. Chappert and V. Mathet, *Microelectron. Eng.*, 2005, **266**, 78–79.
5 P. R. Willmott, *Prog. Surf. Sci.*, 2004, **76**, 163.
6 M. Prestigiacomo, L. Roussel, A. Houel, P. Sudraud, F. Bedu, D. Tonneau, V. Safarov and H. Dellaporta, *Microelectron. Eng.*, 2004, **76**, 175.
7 A. Benninghoven, J. L. Hunter, Jr., B. W. Schueler, H. E. Smith and H. W. Werner, SIMS XIV, Proceedings of the XIVth International Conference on Secondary Ion Mass Spectrometry, *Appl. Surf. Sci.*, **231–232**, 2004.
8 *ToF-SIMS: Surface Analysis by Mass Spectrometry*, ed. J. C. Vickerman and D. Briggs, Surface Spectra/IM Publications, Manchester, 2001.
9 G. Gillen and S. Roberson, *Rapid Commun. Mass Spectrom.*, 1998, **12**, 1303.
10 A. G. Sostarecz, C. M. McQuaw, A. Wucher and N. Winograd, *Anal. Chem.*, 2004, **76**, 6651.
11 C. Szakal, S. Sun, A. Wucher and N. Winograd, *Appl. Surf. Sci.*, 2004, **231–232**, 183.
12 G. Gillen and A. Fahey, *Appl. Surf. Sci.*, 2003, **209**, 203–204.
13 A. Brunelle, S. Della-Negra, J. Depauw, D. Jacquet, Y. Le Beyec, M. Pautrat, K. Baudin and H. H. Andersen, *Phys. Rev. A*, 2001, **63**.
14 D. Weibel, S. Wong, N. Lockyer, P. Blenkinsopp, R. Hill and J. C. Vickerman, *Anal. Chem.*, 2003, **75**, 1754.
15 D. E. Weibel, N. Lockyer and J. C. Vickerman, *Appl. Surf. Sci.*, 2004, **231–232**, 146.
16 J. Xu, C. W. Szakal, S. E. Martin, B. R. Peterson, A. Wucher and N. Winograd, *J. Am. Chem. Soc.*, 2004, **126**, 3902.
17 M. Kerford and R. P. Webb, *Nucl. Instrum. Methods Phys. Res., Sect. B*, 2001, **180**, 44.
18 *Fundamental Processes in Sputtering of Atoms and Molecules Matematisk-fysiske meddelelser 43*, ed. P. Sigmund, Det Kongelige Danske Videnskabernes Selskab, Copenhagen, 1993.
19 G. Marletta, *Nucl. Instrum. Methods Phys. Res., Sect. B*, 1990, **46**, 295.
20 P. Sigmund, in *Sputtering by Particle Bombardment I*, ed. R. Behrisch, Springer, Berlin, 1981, p. 9.
21 M. W. Thompson, *Philos. Mag.*, 1968, **18**, 377.
22 J. F. Ziegler, J. P. Biersack and U. Littmark, *The Stopping and Range of Ions in Solids*, Pergamon Press, New York, 1985.
23 M. T. Robinson, in *Sputtering by Particle Bombardment I*, ed. R. Behrisch, Springer, Berlin, 1981, p. 73.
24 B. J. Garrison, N. Winograd and D. E. Harrison, Jr., *J. Chem. Phys.*, 1978, **69**, 1440.
25 B. J. Garrison, A. Delcorte and K. D. Krantzman, *Acc.Chem. Res.*, 2000, **33**, 69.
26 B. J. Garrison, in *ToF-SIMS: Surface Analysis by Mass Spectrometry*, ed. J. C. Vickerman and D. Briggs, Surface Spectra/IM Publications, Manchester, 2001. p. 223.
27 S. J. Stuart, A. B. Tutein and J. A. Harrison, *J. Chem. Phys.*, 2000, **112**, 6472.
28 D. W. Brenner, *Phys. Rev. B: Condens. Matter*, 1990, **42**, 9458.
29 D. W. Brenner, J. A. Harrison, C. T. White and R. J. Colton, *Thin Solid Films*, 1991, **206**, 220.
30 D. W. Brenner, O. A. Shenderova, J. A. Harrison, S. J. Stuart, B. Ni and S. B. Sinnott, *J. Phys.: Condens. Matter*, 2002, **14**, 783.
31 D. E. Harrison Jr., *CRC Crit. Rev. Solid State Mater. Sci.*, 1988, **14**, S1.
32 N. Winograd and B. J. Garrison, in *Ion Spectroscopies for Surface Analysis*, ed. A. W. Czanderna and D. M. Hercules, Plenum Press, New York, 1991, p. 45.
33 R. Smith, S. D. Kenny and D. Ramasawmy, *Philos. Trans. R. Soc. London, Ser. A*, 2004, **362**, 157–176.
34 K. Beardmore and R. Smith, *Nucl. Instrum. Methods Phys. Res., Sect. B*, 1995, **102**, 223.
35 K. D. Krantzman, Z. Postawa, B. J. Garrison, N. Winograd, S. J. Stuart and J. A. Harrison, *Nucl. Instrum. Methods Phys. Res., Sect. B*, 2001, **180**, 159.
36 Z. Postawa, *Appl. Surf. Sci.*, 2004, **231–232**, 22.
37 Z. Postawa, K. Ludwig, J. Piakowsky, K. Krantzman, N. Winograd and B. J. Garrison, *Nucl. Instrum. Methods Phys. Res., Sect. B*, 2003, **202**, 168.
38 A. Delcorte, P. Bertrand and B. J. Garrison, *J. Phys. Chem. B*, 2001, **105**, 9474.
39 A. Delcorte, B. Arezki, P. Bertrand and B. J. Garrison, *Nucl. Instrum. Methods Phys. Res., Sect. B*, 2002, **193**, 768.
40 A. Delcorte and B. J. Garrison, *J. Phys. Chem. B*, 2003, **107**, 2297.
41 A. Delcorte and B. J. Garrison, *J. Phys. Chem. B*, 2004, **108**, 15652.
42 P. Bertrand and L. T. Weng, *Mikrochim. Acta*, 1996, **13**(Suppl.), 167.
43 B. W. Schueler, *Microsc. Microanal. Microstruct.*, 1992, **3**, 119.
44 K. F. Willey, V. Vorsa, R. M. Braun and N. Winograd, *Rapid Commun. Mass Spectrom.*, 1998, **12**, 1253.
45 R. Chatterjee, D. E. Riederer, Z. Postawa and N. Winograd, *Rapid Commun. Mass Spectrom.*, 1998, **12**, 1227.
46 M. W. Thompson, *Philos. Trans. R. Soc. London, Ser. A*, 2004, **362**, 5–28.
47 R. A. Baragiola, *Philos. Trans. R. Soc. London, Ser. A*, 2004, **362**, 29–53.
48 A. Delcorte, in *ToF-SIMS: Surface Analysis by Mass Spectrometry*, ed. J. C. Vickerman and D. Briggs, Surface Spectra/IM Publications, Manchester, 2001, p. 161.
49 K. Wien, *Nucl. Instrum. Methods Phys. Res., Sect. B*, 1997, **131**, 38.
50 J. P. Biersack, in *Ion Beam Modification of Materials*, ed. P. Mazzoldi and G. W. Arnold, Elsevier, Amsterdam, 1987, p. 648.
51 http://www.srim.org/.
52 A. Delcorte, *Nucl. Instrum. Methods Phys. Res., Sect. B*, 2005, **236**, 1.
53 D. Briggs, in *ToF-SIMS, Surface Analysis by Mass Spectrometry*, ed. J. C. Vickerman and D. Briggs, Surface Spectra/IM Publications, Manchester, 2001, p. 447.
54 F.W. McLafferty and F. Turecek, *Interpretation of Mass Spectra*, University Science Books, Sausalito, 1993.
55 G. J. Leggett, D. Briggs and J. C. Vickerman, *J. Chem. Soc., Faraday Trans.*, 1990, **86**, 1863.
56 G. J. Leggett, J. C. Vickerman, D. Briggs and M. J. Hearn, *J. Chem. Soc., Faraday Trans.*, 1992, **88**, 297.
57 K. A. Cox, J. D. Williams, R. G. Cooks and R. E. Kaiser, *Biol. Mass Spectrom.*, 1992, **21**, 226.
58 G. J. Leggett, in *The Static SIMS Library*, ed. J. C. Vickerman, D. Briggs and A. Henderson, Surface Spectra, Manchester, 1997, p. 19.
59 A. Delcorte, L. T. Weng and P. Bertrand, *Nucl. Instrum. Methods Phys. Res., Sect. B*, 1995, **100**, 213.
60 A. Delcorte, B. G. Segda, B. J. Garrison and P. Bertrand, *Nucl. Instrum. Methods Phys. Res., Sect. B*, 2000, **171**, 277.
61 A. Delcorte and P. Bertrand, *Nucl. Instrum. Methods Phys. Res., Sect. B*, 1996, **115**, 246.
62 A. Delcorte and P. Bertrand, *Nucl. Instrum. Methods Phys. Res., Sect. B*, 1998, **135**, 430.

63 D. E. Riederer, R. Chatterjee, S. W. Rosencrance, Z. Postawa, T. D. Dunbar, D. L. Allara and N. Winograd, *J. Am. Chem. Soc.*, 1997, **119**, 8089.
64 R. M. Papaleo, P. Demirev, J. Eriksson, P. Hakansson, B. U. R. Sundqvist and R. E. Johnson, *Phys. Rev. Lett.*, 1996, **77**, 667.
65 A. Delcorte, X. Vanden Eynde, P. Bertrand, J. C. Vickerman and B. J. Garrison, *J. Phys. Chem. B*, 2000, **104**, 2673.
66 G. J. Leggett and J. C. Vickerman, *Int. J. Mass Spectrom. Ion Processes*, 1992, **122**, 281.
67 I. Gilmore and M. P. Seah, *Surf. Interface Anal.*, 1996, **24**, 746.
68 A. Licciardello, S. Pignataro, A. Leute and A. Benninghoven, *Surf. Interface Anal.*, 1993, **20**, 549.
69 A. Chilkoti, G. P. Lopez, B. D. Ratner, M. J. Hearn and D. Briggs, *Macromolecules*, 1993, **26**, 4825.
70 G. J. Leggett and J. C. Vickerman, *Anal. Chem.*, 1991, **63**, 561.
71 X. Vanden Eynde, H. Oike, M. Hamada, Y. Tezuka and P. Bertrand, *Rapid Commun. Mass Spectrom.*, 1999, **13**, 1917.
72 (*a*) A. Delcorte, B. G. Segda and P. Bertrand, *Surf. Sci.*, 1997, **381**, 18; (*b*) A. Delcorte, B. G. Segda and P. Bertrand, *Erratum: Surf. Sci.*, 1997, **389**, 393.
73 A. Delcorte and P. Bertrand, *Int. J. Mass Spectrom.*, 1999, **184**, 217.
74 A. Schnieders, R. Mollers and A. Benninghoven, *Surf. Sci.*, 2001, **471**, 170.
75 C. A. Meserole, E. Vandeweert, Z. Postawa, B. C. Haynie and N. Winograd, *J. Phys. Chem. B*, 2002, **106**, 12929.
76 N. Médard, A. Benninghoven, D. Rading, A. Licciardello, A. Auditore, Tran Minh Duc, H. Montigaud, F. Vernerey, C. Poleunis and P. Bertrand, *Appl. Surf. Sci.*, 2003, **203–204**, 571.
77 K. D. Krantzman, Z. Postawa, B. J. Garrison, N. Winograd, S. J. Stuart and J. A. Harrison, *Nucl. Instrum. Methods Phys. Res., Sect. B*, 2001, **180**, 159.
78 C. A. Meserole, E. Vandeweert, Z. Postawa and N. Winograd, *J. Phys. Chem. B*, 2004, **108**, 15686.
79 J. Sunner, *J. Org. Mass Spectrom.*, 1993, **28**, 805.
80 A. Benninghoven, W. Lange, M. Jirikowski and D. Holtkamp, *Surf. Sci.*, 1982, **123**, L721.
81 S. Tamaki, W. Sichtermann and A. Benninghoven, *Jpn. J. Appl. Phys.*, 1984, **23**, 544.
82 J.-X. Li and J. A. Gardella, *Anal. Chem.*, 1994, **66**, 1032.
83 A. Delcorte and P. Bertrand, *Surf. Sci.*, 1998, **412/413**, 97.
84 *Ion Formation from Organic Solids*, ed. A. Benninghoven, Springer, Berlin, 1982. p. 64.
85 R. G. Cooks and K. L. Bush, *Int. J. Mass Spectrom. Ion Phys.*, 1983, **53**, 111.
86 A. Spool, *Surf. Interface Anal.*, 2004, **36**, 264.
87 A. Wucher, M. Wahl and H. Oechsner, in *Secondary Ion Mass Spectrometry SIMS IX*, ed. A. Benninghoven, Y. Nihei, R. Shimizu and H. W. Werner, Wiley, New York, 1993, p. 100.
88 V. Solomko, A. Delcorte, B. J. Garrison and P. Bertrand, *Appl. Surf. Sci.*, 2004, **231–232**, 48.
89 K. L. Busch, B. H. Hsu, Y.-X. Xie and R. G. Cooks, *Anal. Chem.*, 1983, **55**, 1157.
90 H. Grade, N. Winograd and R. G. Cooks, *J. Am. Chem. Soc.*, 1977, **99**, 7725.
91 H. Grade and R. G. Cooks, *J. Am. Chem. Soc.*, 1978, **100**, 5615.
92 I. V. Bletsos, D. M. Hercules, D. van Leyen and A. Benninghoven, *Macromolecules*, 1987, **20**, 407.
93 B. Hagenhoff, M. Deimel, A. Benninghoven, H.-U. Siegmund and D. Holtkamp, *J. Phys. D: Appl. Phys.*, 1992, **25**, 818.
94 Th. J. Colla, R. Aderjan, R. Kissel and H. M. Urbassek, *Phys. Rev. B: Condens. Matter*, 2000, **62**, 8487.
95 G. Betz and W. Husinsky, *Philos. Trans. R. Soc. London, Ser. A*, 2004, **362**, 177.
96 A. Delcorte and B. J. Garrison, *J. Phys. Chem. B*, 2000, **104**, 6785.
97 B. Arezki, A. Delcorte and P. Bertrand, *Nucl. Instrum. Methods Phys. Res., Sect. B*, 2002, **193**, 755.
98 B. Arezki, A. Delcorte, A. C. Chami, B. J. Garrison and P. Bertrand, *Nucl. Instrum. Methods Phys. Res., Sect. B*, 2003, **212**, 755.
99 B. Arezki, A. Delcorte and P. Bertrand, *Appl. Surf. Sci.*, 2004, **231–232**, 122.
100 B. Arezki, A. Delcorte, P. Bertrand and B. J. Garrison, *J. Phys. Chem. B*, 2005, submitted.
101 K. J. Wu and R. W. Odom, *Anal. Chem.*, 1996, **68**, 873.
102 K. Wittmaack, W. Szymczak, G. Hoheisel and W. Tuszynski, *J. Am. Soc. Mass Spectrom.*, 2000, **11**, 553.
103 S. L. Luxembourg, L. A. McDonnell, M. C. Duursma, X. H. Guo and R. M. A. Heeren, *Anal. Chem.*, 2003, **75**, 2333.
104 L. Adriaensen, F. Vangaever, J. Lenaerts and R. Gijbels, *Rapid Commun. Mass Spectrom.*, 2005, **19**, 1017.
105 K. Tanaka, H. Waki, Y. Ido, S. Akita, Y. Yoshida and T. Yoshida, *Rapid Commun. Mass Spectrom.*, 1988, **2**, 151.
106 M. Karas, D. Bachmann, U. Bahr and F. Hillenkamp, *Int. J. Mass Spectrom. Ion Processes*, 1988, **78**, 53.
107 A. Delcorte, N. Médard and P. Bertrand, *Anal. Chem.*, 2002, **74**, 4955.
108 A. Delcorte, B. Arezki and B. J. Garrison, *Nucl. Instrum. Methods Phys. Res., Sect. B*, 2003, **212**, 414.
109 A. I. Gusev, B. K. Choi and D. M. Hercules, *J. Mass Spectrom.*, 1998, **33**, 480.
110 A. Delcorte and P. Bertrand, *Anal. Chem.*, 2005, **77**, 2107.
111 I. Wojciechowski, A. Delcorte, X. Gonze and P. Bertrand, *Chem. Phys. Lett.*, 2001, **346**, 1.
112 A. Delcorte, I. Wojciechowski, X. Gonze, B. J. Garrison and P. Bertrand, *Int. J. Mass Spectrom.*, 2002, **214**, 213.
113 N. Winograd, *Anal. Chem.*, 2005, **77**, 143A.
114 M. Van Stipdonk, in *ToF-SIMS: Surface Analysis by Mass Spectrometry*, ed. J. C. Vickerman and D. Briggs, Surface Spectra/IM Publications, Chichester, 2001, ch. 12.
115 Z. Postawa, B. Czerwinski, M. Szewczyk, E. J. Smiley, N. Winograd and B. J. Garrison, *Anal. Chem.*, 2003, **75**, 4402.
116 S. Sun, C. Szakal, E. J. Smiley, Z. Postawa, A. Wucher, B. J. Garrison and N. Winograd, *Appl. Surf. Sci.*, 2004, **231–232**, 64.
117 A. Delcorte, M. Henry, C. Poleunis and P. Bertrand, contribution presented at the 16th European Symposium on Polymer Spectroscopy (ESOPS2005), Kerkrade, The Netherlands, June, 2005.
118 Z. Postawa, *Appl. Surf. Sci.*, 2004, **231–232**, 22.
119 M. K. Miller, K. F. Russell and G. B. Thompson, *Ultramicroscopy*, 2005, **102**, 287.
120 G. Chai, L. Chow, D. Zhou and S. R. Byahut, *Carbon*, 2005, in press.
121 B. Schaffer, C. Mitterbauer, A. Schertel, A. Pogantsch, S. Rentenberger, E. Zojer and F. Hofer, *Ultramicroscopy*, 2004, **101**, 123.
122 F. Z. Cui and Z. S. Luo, *Surf. Coat. Technol.*, 1999, **112**, 278.
123 R. Antony, B. Lucas, B. Ratier and A. Moliton, *Synth. Met.*, 1999, **102**, 908.
124 C. Satriano, N. Spinella, M. Manso, A. Licciardello, F. Rossi and G. Marletta, *Mater. Sci. Eng., C*, 2003, **23**, 779.
125 G. Marletta, G. Ciapetti, C. Satriano, S. Paganini and N. Baldini, *Biomaterials*, 2005, **26**, 4793.
126 P. Bertrand, P. Lambert and Y. Travaly, *Nucl. Instrum. Methods Phys. Res., Sect. B*, 1997, **131**, 71.
127 K. Wang, O. Schneegans, A. Moradpour and F. Jomard, *Appl. Phys. Lett.*, 2004, **85**, 5878.
128 H. Omichi, *Nucl. Instrum. Methods Phys. Res., Sect. B*, 1995, **105**, 302.
129 G. Marletta, Andras Toth, Imre Bertoti, Tran Minh Duc, F. Sommerd and K. Ferencz, *Nucl. Instrum. Methods Phys. Res., Sect. B*, 1998, **141**, 684.
130 S. Brunner, D. M. Ruck, K. Tinschert, W. F. X. Frank and B. Knodler, *Nucl. Instrum. Methods Phys. Res., Sect. B*, 1996, **107**, 333.
131 A. L. Stepanov and R. I. Khaibullin, *Rev. Adv. Mater. Sci.*, 2004, **7**, 108.
132 S. N. Abdullin, A. L. Stepanov, Yu. N. Osin, R. I. Khaibullin and I. B. Khaibullin, *Surf. Coat. Technol.*, 1998, **106**, 214.
133 C. Xirouchaki and R. E. Palmer, *Vacuum*, 2002, **66**, 167.
134 J. Cheng and N. Winograd, *Anal. Chem.*, 2005, **77**, 3651.
135 S. Sun, A. Wucher, C. Szakal and N. Winograd, *Appl. Phys. Lett.*, 2004, **84**, 5177.
136 Z. Postawa, B. Czerwinski, N. Winograd and B. Garrison, *J. Phys. Chem. B*, 2005, **109**, 11973.
137 F. Kollmer, *Appl. Surf. Sci.*, 2004, **231–232**, 153.
138 B. Hagenhoff, K. Pfitzer, E. Tallarek, R. Koch and R. Kersting, *Appl. Surf. Sci.*, 2004, **231–232**, 196.

